State-resolved investigation of the photodesorption dynamics of NO from $(NO)_2$ on Ag nanoparticles of various sizes in comparison with Ag(111)

Daniel Mulugeta, Kazuo Watanabe,[a] Dietrich Menzel,[b] and Hans-Joachim Freund
Fritz-Haber-Institute der Max-Planck Gesellschaft, Faradayweg 4–6, 14159 Berlin, Germany

(Received 8 December 2010; accepted 2 April 2011; published online 29 April 2011)

The translational and internal state energy distributions of NO desorbed by laser light (2.3, 3.5, and 4.7 eV) from adsorbed $(NO)_2$ on Ag nanoparticles (NPs) (mean diameters, $D = 4$, 8, and 11 nm) have been investigated by the $(1 + 1)$ resonance enhanced multiphoton ionization technique. For comparison, the same experiments have also been carried out on Ag(111). Detected NO molecules are hyperthermally fast and both rotationally and vibrationally hot, with temperatures well above the sample temperature. The translational and rotational excitations are positively correlated, while the vibrational excitation is decoupled from the other two degrees of freedom. Most of the energy content of the desorbing NO is contained in its translation. The translational and internal energy distributions of NO molecules photodesorbed by 2.3, 3.5, and in part also 4.7 eV light are approximately constant as a function of Ag NPs sizes, and they are the same on Ag(111). This suggests that for these excitations a common mechanism is operative on the bulk single crystal and on NPs, independent of the size regime. Notably, despite the strongly enhanced cross section seen on NP at 3.5 eV excitation energy in *p*-polarization, i.e., in resonance with the plasmon excitation, the mechanism is also unchanged. At 4.7 eV and for small particles, however, an additional desorption channel is observed which results in desorbates with higher energies in all degrees of freedom. The results are well compatible with our earlier measurements of size-dependent translational energy distributions. We suggest that the broadly constant mechanism over most of the investigated range runs via a transient negative ion state, while at high excitation energy and for small particles the transient state is suggested to be a positive ion. © *2011 American Institute of Physics*. [doi:10.1063/1.3581802]

I. INTRODUCTION

Understanding of elementary processes on surfaces is a key issue in photochemistry of molecules for both fundamental and practical reasons. Photoinduced desorption of molecules is the simplest surface reaction driven by photons. Studies of these processes under ultrahigh vacuum (UHV) conditions on well defined single crystal surfaces, often utilizing simple test adsorbates such as CO and NO, have been the major focus in the past decades.[1–4] Electronically driven desorption processes usually lead to hyperthermal energies in the products which can be investigated by state-resolved measurements of the distribution of energy over the molecular degrees of freedom (DOF) of desorbing molecules, translation, rotation, and vibration.[1–3] These energy distributions are intimately connected with the mechanistic steps, the excitation and relaxation processes, and the motion of the representative wave packets on the potential energy surfaces (PESs) of the excited and the ground states. They are typically interpreted in terms of basic semiclassical models (of which the oldest is the Menzel-Gomer-Redhead (MGR) model[5]) or, if sufficient information is available, by sophisticated theoretical calculations.[3,6]

However, results from studies on flat single crystal surfaces are not necessarily transferable to surface photochemistry on more complex materials, such as nanoparticles (NPs). Interesting photochemical effects of NPs do not only derive from their increased surface/volume ratio, but also from their unique optical, electronic, and catalytic properties which can be tuned by size, shape, and/or support material.[7–9] In particular, the optical properties of metal nanoparticles (MNPs), which are often dominated by the so called Mie plasmon excitation, are rather well understood.[7–9] Nevertheless, the number of experimental investigations that address the effects of size and/or plasmon excitation on the photochemistry of adsorbates on MNP surfaces is very limited. Plasmon-induced enhancement of the photoreactivity of adsorbates via field enhancement on roughened metal surfaces[10,11] and on MNPs (Refs. 9, 12, and 13) or composite materials composed of MNPs (Ref. 14) has been reported. Even a direct influence of plasmon excitation on the photodesorption of Xe on alumina-supported Ag NPs has been observed.[15] Size effects have been seen as well.[12,13,16] Apart from the plasmon excitation, confinement of the electronic excitations within the nanometer-sized MNPs can be important, for instance, via influencing the number and/or evolution of photoproduced hot electrons,[17–20] which may correspondingly change the efficiency of photoinduced processes and lead to size dependences.[9,13,19]

To improve our understanding of these photochemical effects of NPs, we follow the strategy to compare experimental results for a prototypical photochemical process on NPs as a

[a]Present address: Department of Chemistry, Tokyo University of Science, 1–3 Kagurazaka, Shinjuku-ku, Tokyo 162–8601, Japan.
[b]Also at Physik-Department E20, Technische Universität München, 85747 Garching, Germany. Electronic mail: dietrich.menzel@ph.tum.de.

function of particle size, and for the surface of a bulk crystal of the same material, using various primary excitations. As a model system we have chosen NO adsorbed on Ag NPs of varying sizes and on Ag(111). It is known from extensive experimental and theoretical studies[11,21] that at sample temperatures below 77 K which are needed for adsorption of NO on Ag(111), NO forms adsorbed dimers. Upon heating or photon irradiation of the surface, the dimer partially dissociates to (partly desorbing) NO monomers, or reacts to form adsorbed N_2O and O. Quite similar behavior of NO adsorption was observed on Ag and NP surfaces.[13] Previous work has reported on cross sections and translational energies of photodesorbed NO obtained by mass-selected time-of-flight (MS-TOF) measurements yielding translational energies expressed as translational temperatures on Ag(111)[22] and on Ag NPs of varying size.[13,23] In the present paper, we report on detailed internal energy distributions (rotations and vibrations) of desorbing NO obtained by the resonance enhanced multiphoton ionization (REMPI) method, for Ag(111) and for Ag NPs of varying size, in order to fully characterize the dynamics in this system and their dependence on size and excitation.

II. EXPERIMENTAL

The experiments were carried out in two vertically connected UHV chambers described previously. Briefly, the upper chamber was equipped with standard instruments for checking surface morphology, cleanliness, and residual gas pressure as described elsewhere.[13,22,23] The lower chamber could be alternatively equipped with MS-TOF, REMPI, and two-photon photoemission spectroscopy[24] detectors. Here we used the REMPI setup.

For details of sample cleaning and nanoparticle preparation, see Refs. 25–27. Briefly, thin alumina films on a NiAl (110) surface were used as support for Ag NPs. Daily preparation included cleaning the NiAl (110) crystal, preparing a thin oxide film on it, and depositing Ag atoms on the oxide film evaporated from a molybdenum crucible (at an Ag atom flux of 1 Å/min, calibrated by a quartz microbalance) at room temperature, to form the Ag NPs according to procedures developed in this institute.[25] Since the Ag NPs nucleate only on surface defects whose density can be controlled by the preparation of the oxide film, the NP mean size (± 20 to 30%) is given by the amount of evaporated Ag. The samples were attached to a cryostat coolable by liquid helium and were cooled to 30–40 K for photodesorption experiments. Heating was accomplished either by radiation (<700 K) or by electron bombardment from a tantalum filament mounted behind the crystal (>700 K). The sample temperature was monitored by type-E chromel-constantan thermocouples spotwelded to the sides of the crystal. The Ag(111) crystal was mounted similarly and cleaned by established procedures.[22]

The sample surface was dosed with NO molecules by backfilling the chamber to a static pressure using a manual leak valve. Photodesorption was initiated with the second, third, or forth harmonic of an Nd-YAG laser at 2.3, 3.5, or 4.7 eV, at pulse durations of about 5 ns and a repetition rate of 10 Hz. Pulse fluences of 0.5–2 mJ/cm^2 were used. We stress that in this time/fluence regime all desorption effects are strictly linear; much higher photon densities are necessary to cause nonlinear effects.[26] In order to perform desorption at a high, constant NO coverage the crystal was kept at 60 K and continuously dosed with a background NO pressure of 5×10^{-9} to 4×10^{-8} mbar (depending on the laser energy, fluence, polarization, and desorption cross section of NO) during the photodesorption experiment. The background pressure was adjusted such that the REMPI signal stayed constant, keeping the dimer layer close to saturated. This procedure ensures that the signal is dominated by photodesorption from NO dimers.[13,22] No evidence of any accumulation of impurities (by temporal changes of measured parameters or postirradiation thermal desorption) was seen during the measurements which in some cases had to be extended for sufficient signal/noise ratio. Agreement of the earlier MS-TOF spectra[13] with the REMPI-TOF spectra obtained here (see below) further corroborate this conclusion. Desorbed NO molecules were detected state selectively by (1 + 1)-REMPI via the $A\ ^2\Sigma\ (v' = 0, 1) \leftarrow X^2\Pi\ (v'' = 0, 1)$ transitions,[28] at a distance of 27 mm from the surface (spot size ~2 mm). For detection, tunable ultraviolet (UV) radiation between 216 and 237 nm (linewidth 0.3 cm^{-1}, pulse energy ~1.5 mJ, and pulse duration ~15 ns) was obtained by frequency doubling with a β-barium borate crystal of an excimer laser-pumped dye laser system operating at 432–474 nm with Coumarine-2 dyes. A computer-controlled motorized filter wheel with various neutral density filters was used to keep the probe laser energy roughly constant and at sufficiently low values to avoid saturation effects. The resulting ions were accelerated toward a multichannel plate assembly by a repeller plate held at +1 kV and detected as an ion current.

The REMPI signal obtained without desorption laser pulse gives the background signal, while the REMPI signal after photodesorption consists of the sum of the background and photodesorbed NO signal. After background subtraction, the REMPI signal is normalized with respect to the pump and probe laser powers according to their power relations. For further details see Ref. 27.

III. RESULTS

A. Translational energy distributions

Quantum state resolved TOF spectra of photodesorbed NO molecules (REMPI-TOF spectra) were obtained by plotting the ion signal (at a known rovibrational transition) as a function of pump-probe laser delay, Δt (with Δt varied between 0 and 300 μs). The translational energy distributions for each internal state were obtained by fitting the resulting REMPI-TOF spectra with a flux-weighted, shifted Maxwell–Boltzmann (SMB) distribution, $f(t) = a/t^4 \exp\left(-b(L/t - v_0)^2\right)$, corrected for the decrease in detection efficiency with velocity as has been done before for the MS-TOF spectra.[13] Here a, b are the parameters of amplitude and spread, respectively, t is the flight time of desorbate, L is the flight length (~27 mm), and v_0 is the parameter related to the shift from the thermal Maxwell–Boltzmann distribution.[3] The mean translational energy was obtained by numerical integration of the

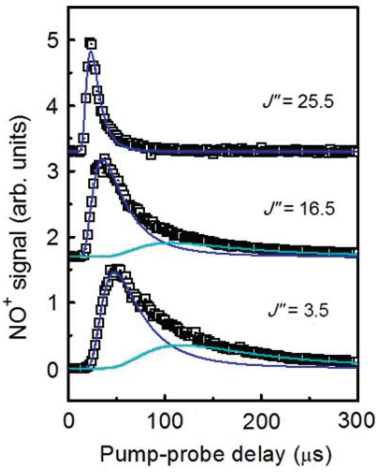

FIG. 1. TOF spectra for three different rotational states, J'', of NO ($v'' = 0$, $\Omega'' = X^2\Pi_{1/2}$) photodesorbed from 8 nm Ag NPs at $h\nu = 2.3$ eV. The solid lines are fits to the shifted Maxwell–Boltzmann distribution. At lower J'' a slow contribution of thermal and/or scattered molecules is seen and can be fitted with another SMB (light lines).

fitted function and can then be expressed by the translational temperature, $T_{tr} = <E_{tr}>/2k_B$, where k_B is the Boltzmann constant.

Figure 1 shows an example of a series of REMPI-TOF spectra measured from NO (for vibrations $v'' = 0$, spin state $\Omega'' = \frac{1}{2}$, and various rotational states J''; many other parameter combinations were recorded[27]), photodesorbed by 2.3 eV p-polarized photons from $(NO)_2$ adsorbed on 8 nm Ag NPs. NO molecules photodesorbed with lower J'' have broader TOF spectra which are well fitted by the sum of two SMB distributions, a fast and a slow (close to the sample temperature of 60 K) channel. We ascribe them to photochemical desorption and to scattered or thermally desorbed molecules, respectively. The contribution of the latter channel decreases quickly with increasing J'' and disappears for higher J'' states. In parallel, the fast TOF component becomes narrower and shifts to earlier pump–probe delays with increasing J''. In contrast to this J'' dependence of the translational energy, no dependence of translational or rotational energy of desorbed NO on vibrational excitation is observed: for molecules in $v'' = 0$ or 1, identical translational/rotational spectra are obtained, as will be discussed in more detail below. The same behavior—rotation and translation positively coupled, vibration decoupled—was observed for NO molecules desorbed from other NP sizes or from Ag(111), and for the other photon energies used in this work, even for a parameter set (4.7 eV, small NPs) which yields distinctly different individual parameters (see below).

B. Internal (rotational, vibrational, and spin–orbit) state energy distributions

The rotational state distributions of photodesorbed NO were extracted from the intensity distributions of the REMPI spectra measured at a fixed Δt (i.e., for a fixed velocity) after weighting them with degeneracy and line strength (Hönl-London) factors.[3,28,29] Figure 2 shows typical data with (a)

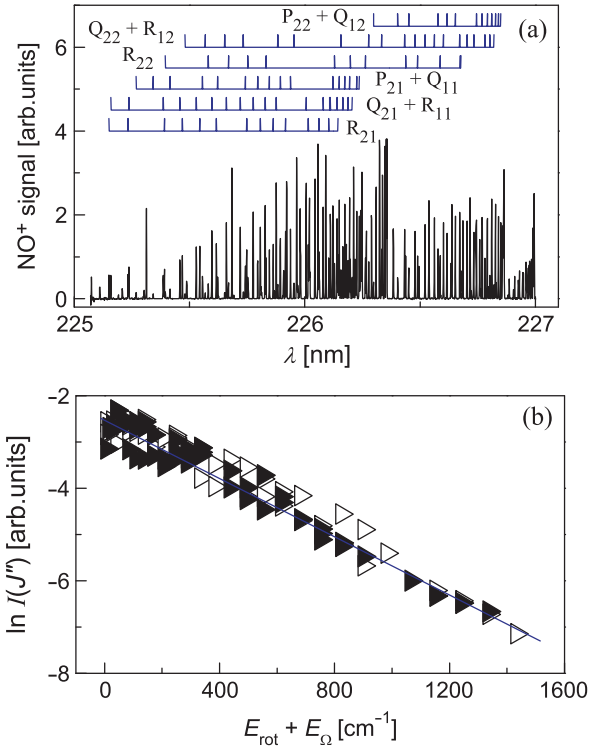

FIG. 2. (a) Typical (1+1) REMPI spectrum of NO ($v'' = 0$, $\Delta t = 29$ μs) desorbed with 3.5 eV photons in p-polarization from 8 nm Ag NPs. (b) Boltzmann plot of the rotational distribution of NO ($v'' = 0$, $\Delta t = 29$ μs) desorbed with 3.5 eV photons in p-polarization from 8 nm Ag NPs. Empty triangles: $\Omega'' = X^2\Pi_{1/2}$, filled triangles: $\Omega'' = X^2\Pi_{3/2}$.

a REMPI spectrum measured from NO ($v'' = 0$, velocity = 950 m/s; again many additional conditions were examined[27]) desorbed from 8 nm Ag NPs with p-polarized photons of 3.5 eV and (b) the corresponding Boltzmann plot. The latter is characterized by a single straight line in the given units (i.e., by a thermal rotational distribution), which yields a rotational temperature of $T_{rot} = \sim 485$ K. The contributions from the two spin–orbit states ($X^2\Pi_{1/2}$ and $X^2\Pi_{3/2}$), which are energetically separated by about 124 cm^{-1}, fall along the same line in the Boltzmann plots which suggests that the spin–orbit excitations are in equilibrium with the rotational excitations.

The vibrational temperatures (T_{vib}) were estimated by comparing the signal intensities in $v'' = 1$ and $v'' = 0$ states with similar J'', after intensity normalization with Franck–Condon factors (0.17 and 0.11 for the (0,0) and (1,1) NO transitions, respectively[29]), assuming a Boltzmann distribution and equal detection efficiencies for the $v'' = 0$ and 1 states.

The REMPI-TOF spectra were recorded from various Ag NP sizes and excitation photon energies and the corresponding T_{rot} and T_{vib} were determined. Figures 3 and 4 collect the data in pseudo-3D plots. Table I lists the numerical values. As can be seen the results for mean translational, rotational, and vibrational energy content of the desorbing molecules are essentially constant, independent of excitation energy, and particle size (including Ag(111): $1/R = 0$), with one notable exception. The delay time-dependent spectra of pho-

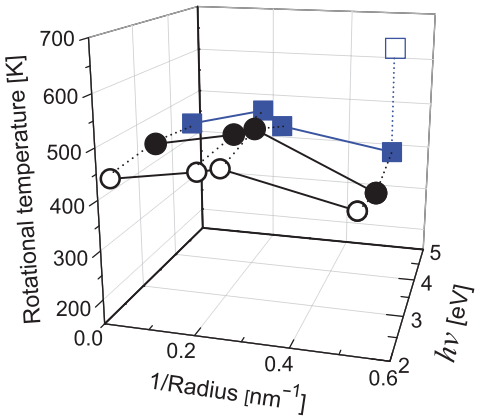

FIG. 3. Pseudo-3D plot of the mean rotational excitation (given as the rotational temperature) of desorbed NO, as functions of excitation energy and particle size (given as inverse radius, $1/R$, including Ag(111) at $1/R = 0$). Very little variation is seen except for 4.7 eV excitation and smallest size (4 nm or $1/R = 0.5$ nm^{-1}), where slow molecules show normal rotational excitation (filled square), while this is much higher for fast molecules (empty square).

todesorbed NO measured from *small* Ag NPs ($D = 4$ nm) at $h\nu = 4.7$ eV were found to exhibit an additional faster component compared to results measured from larger particles or Ag(111) at 4.7 eV, and for all samples and lower photon energies (see Figs. 3 and 4). This finding corroborates the results of the REMPI-TOF measurements above and also those of the previous MS-TOF measurements which had investigated more NP sizes.[13] At this special condition (high excitation energy, very small particles) considerably changed final state energies are found, with higher energies in all DOF (Figs. 3–5). In Ref. 13, we have interpreted this as the opening of a new channel for these conditions; we will return to the interpretation below. To characterize it and separate it from the normal photochemical channel as far as possible, we have measured REMPI spectra at two different Δt which contain strong contributions from one or the other of the two chan-

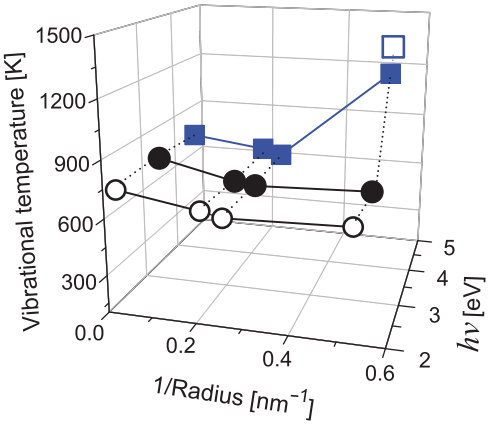

FIG. 4. Pseudo-3D plot of the mean vibrational excitation (given as vibrational temperature) of desorbed NO, as functions of excitation energy and particle size (given as inverse radius, $1/R$, including Ag(111) at $1/R = 0$). Very little variation is seen except for 4.7 eV excitation and the smallest size (4 nm or $1/R = 0.5$ nm^{-1}), for which very fast NO (1500 m/s, empty square) shows very high vibration, but also slow NO (filled square) possesses higher vibrations than all the other conditions (see text for discussion).

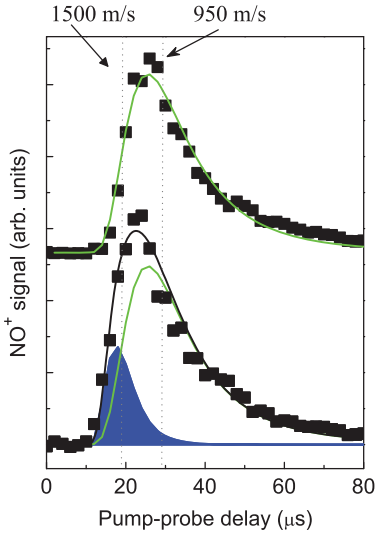

FIG. 5. REMPI-TOF spectra of photodesorbed NO ($v'' = 0, J'' = 25.5, \Omega'' = X^2\Pi_{1/2}$ state) measured from 8 (upper spectrum) and 4 nm (lower spectrum) Ag NPs at $h\nu = 4.7$ eV. The lower spectrum for 4 nm NPs is decomposed into the sum of two SMB functions, first with the shape of the 8 nm TOF spectrum (light line), and the remaining fast component is fitted with a second SMB function (blue filled area). The vertical dotted lines on the TOF spectrum show the velocities for which rotational and vibrational distributions were obtained.

nels. The REMPI signal at $\Delta t = 29$ μs (velocity ~950 m/s) is dominated by the internal state population distribution of the *normal, slower* component, while the internal state population distribution of the new, *faster* component was maximized by measuring the REMPI spectrum at a shorter Δt, 19 μs (i.e., molecules with a velocity of ~1500 m/s) where it is strong (though not dominant). As shown in Fig. 6 the correlation of translation and rotation also exists for the new component, albeit with a distinctly higher gradient.

Table I collects the rotational and vibrational temperatures of photodesorbed NO measured for various Ag NP sizes and Ag (111) for $h\nu = 2.3$, 3.5, and 4.7 eV contained in Figs. 3 and 4. Errors (estimated from reproducibility) are

TABLE I. Summary of the rotational and vibrational temperatures of NO photodesorbed with 2.3, 3.5, and 4.7 eV from Ag NP surfaces of varied size. The results from Ag(111) are also shown for comparison.

$h\nu$ (ev)	Polarization	Substrate	Velocity (m/s)	T_{rot}(K)	T_{vib} (K)
2.3	*p*	Ag (111)	950	425	780
	p	4 nm Ag NPs	950	405	692
	p	8 nm Ag NPs	950	462	667
	p	11 nm Ag NPs	950	452	697
3.5	*p*	Ag (111)	950	438	797
	p	4 nm Ag NPs	950	370	687
	p	8 nm Ag NPs	950	485	655
	s	8 nm Ag NPs	950	490	700
	p	11 nm Ag NPs	950	470	670
4.7	*p*	Ag (111)	950	432	788
	p	4 nm Ag NPs	950	400	1390
	p	4 nm Ag NPs	1500	620	1540
	p	8 nm Ag NPs	950	440	686
	p	11 nm Ag NPs	950	474	726

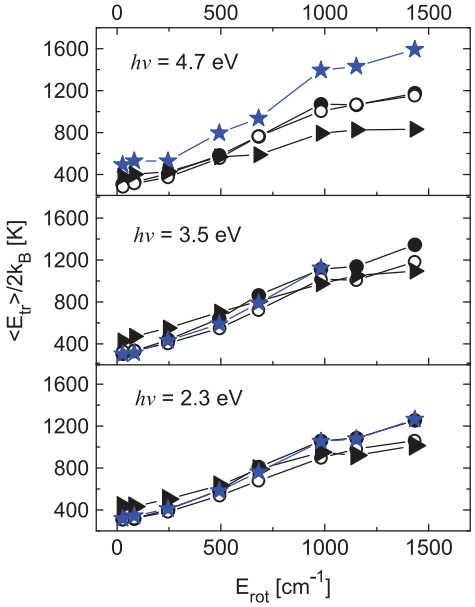

FIG. 6. Correlation between translation and rotation for the three excitation energies used, as indicated. Mean translational energy, given by the translational temperature, $T_{tr} = \langle E_{tr}\rangle/2k_B$, is plotted as a function of rotational energy of NO ($v'' = 0$, $\Omega'' = X^2\Pi_{1/2}$), desorbed with $h\nu = 4.7$ eV from 4 nm Ag NPs (filled stares), 8 nm Ag NPs (filled circles), 11 nm Ag NPs (empty circles), and Ag (111) (filled triangles). In all cases roughly linear correlations are found, which are about identical for all conditions except for 4 nm at 4.7 eV, where consistently higher excitations result.

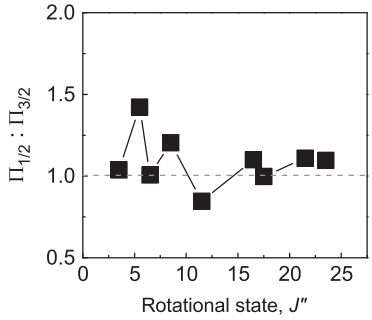

FIG. 7. Individual population ratios for the spin–orbit $\Pi_{1/2}$ and $\Pi_{3/2}$ states of NO desorbed from 8 nm Ag NPs at $h\nu = 3.5$ eV (p-pol.) at various rotational states, J''.

about ± 50 K. At $h\nu = 2.3$, 3.5, and 4.7 eV, the T_{rot} of photodesorbed NO with a velocity of 950 m/s is almost constant (within the experimental error) at ~450 ± 50 K throughout the D range and including Ag(111). However, those molecules desorbed with a velocity of 1500 m/s (fast component) from 4 nm Ag NPs with 4.7 eV have a clearly higher T_{rot}, ~620 K.

Similarly, at 2.3 and 3.5 eV the vibrational level v" = 1 is populated with ~2%–3% of the photodesorbed molecules, which corresponds to a T_{vib} of ~700–800 K and does not significantly change with D. On the other hand, at 4.7 eV and for $D = 4$ nm Ag NPs the vibrational level $v'' = 1$ is populated with ~14% (T_{vib} ~1390 K) for the normal, slower component of photodesorbed NO and ~17% (T_{vib} ~1550 K) for the faster one. At 4.7 eV excitation even the slower component shows a somewhat increased vibrational excitation. One possible reason could be that there is sufficient extension of the distribution of the "new" channel down to this velocity in the $v'' = 1$ state (although the decomposition in Fig. 5 makes this doubtful). Since there is no coupling of translation and vibration, selection of the velocity does not select the vibrational excitation for the fast or slow molecules.

In view of the strong effect of plasmon excitation on the photodesorption cross section,[13,23] it is particularly interesting to check for an effect of plasmon excitation on the rotational and vibrational energy distributions of the photodesorbed NO molecules. We therefore carried out REMPI measurements with photons *on*-resonance (3.5 eV in *p*-polarization) and *off*-resonance (3.5 eV in *s*-polarization) of the (1,0) plasmon. For these two cases the cross sections differ by a factor of ~8 for 8 nm Ag NPs (Ref. 13). The T_{rot} and T_{vib} of photodesorbed NO molecules measured from 8 nm Ag NPs were found to be ~485 K and ~660 K at $h\nu = 3.5$ eV in *p*-polarization, and ~490 K and ~700 K at $h\nu = 3.5$ eV in *s*-polarization, respectively; i.e., they were about the same. Similarly, the state resolved translational temperature of photodesorbed NO does not change significantly between *p*- and *s*-polarization, as shown in Table II. These observations show that the plasmon excitation has no significant influence on the rotational and vibrational excitations of the photodesorbed molecules, corroborating the earlier finding of unchanged translational energies on and off the plasmon resonance.[13] The conclusion of unchanged mechanism is thereby reinforced.

The REMPI spectra obtained from a wavelength scan can also probe the populations in the two spin–orbit states of the ground state of NO [an example has already been shown in Fig. 2(b)]. The spin–orbit state population can be determined by comparing the peak heights (after normalizing with the Hönl-London factors) for transitions originating in $X^2\Pi_{1/2}$ and $X^2\Pi_{3/2}$ spin states. Figure 7 shows the individual population ratios in the spin–orbit $\Pi_{1/2}$ and $\Pi_{3/2}$ states as a function of J'' of NO desorbed from 8 nm Ag NPs at $h\nu = 3.5$ eV (p-pol.). As can be seen from the figure the two spin–orbit states are always roughly equally populated, although some fluctuations occur.

C. Energy partitioning

From the energy provided by the photon, $h\nu$, a part will be needed for dimer dissociation and subsequent breaking of the adsorption bond. The remainder will be available for excitations of translational and internal DOF of the desorbed NO, as well as for dissipation into the substrate. Due to the weak dimer[30] and adsorption (derived from thermal desorption) bonds (of about 0.1–0.15 eV each), the first part is small (~0.2–0.3 eV) and constant for varied excitation.

The total energy in the translational and internal DOF of the desorbed NO molecules can be determined from the translational and internal energy distributions presented above. The average translational energies of photodesorbed NO molecules have been taken from the MS-TOF measurements.[13] Since these measurements are already

TABLE II. Comparisons between the translational temperature of NO ($v'' = 0$, $\Omega'' = X^2\Pi_{1/2}$) photodesorbed with 3.5 eV in *p*-polarization (*on*-plasmon resonance) and in *s*-polarization (*off*-plasmon resonance) from 8 nm Ag NPs.

	$v'' = 0, \Omega'' = 1/2$			
	$J'' = 3.5$	$J'' = 16.5$	$J'' = 23.5$	$J'' = 28.5$
T_{tr} at $h\nu = 3.5$ eV, *p*-pol.	304 K	640 K	1111 K	1345 K
T_{tr} at $h\nu = 3.5$ eV, *s*-pol.	291 K	577 K	1056 K	1262 K

averaged over the internal quantum states, no further averaging is necessary. An *average* rotational energy, $\langle E_{rot}(v'')\rangle$, of the photodesorbed NO in a specific vibrational state, can be obtained by calculating a weighted average sum, $\langle E_{rot}(v'')\rangle = (1/N(v'')) \sum_J N_{rot}(v'', J'') E_{rot}(v'', J'')$, between $J'' = 3.5$ and 28.5, where N_{rot} denotes the population of the rotational level with energy E_{rot}. The total rotational energy has to be weighted by the vibrational population for the $v'' = 0$, and $v'' = 1$ states (higher vibrational states can be safely neglected). We stress that there may be errors in the result since we determine the *average* rotational energies only for molecules desorbed at a specific velocity. Due to the translation–rotation coupling, these *average* energies may not represent the total average rotational energy of the entire velocity distributions. This means that the actual mean rotational energy may be somewhat larger. Similarly, the average vibrational energy,$\langle E_{vib}\rangle$, of photodesorbed NO can be calculated by using $\langle E_{vib}\rangle = (1/N) \sum_v N_{vib}(v'') E_{vib}(v'')$, where $E_{vib}(v'')$ is the vibrational state energy and $N_{vib}(v'')$ is the population of the corresponding vibrational level ($v'' = 0$ or 1).

The results found for the individual average energies which go to the different DOF of the desorbate are summarized in Table III. The total energy $\langle E_{tot}\rangle$ can then be obtained from the sum of the contributions of all DOF:$\langle E_{tot}\rangle = \langle E_{tr}\rangle + \langle E_{rot}\rangle + \langle E_{vib}\rangle$. As can be seen from Table III, only small fractions of the available energy are released into the photodesorbed NO molecules (~0.17 eV for the normal, slower component and ~0.51 eV for the fastest component). So the major part of the primary excitations will be dissipated in the substrate, partly by recoil and partly by returning hot electrons (see Sec. IV). In addition, the energy is not equally partitioned into the different DOF of the desorbing NO: the majority of the energy goes into the translation. This conclusion is not changed by a possible error in the determination of the mean rotational anergy discussed above.

D. Correlations

In addition to the individual final state energy distributions, knowledge of the correlations between them is very important for conclusions about the dynamics of the desorption process and for comparison with calculations. Evaluation of the mean translational energy of photodesorbed NO from the measured TOF spectra at various J'' have been shown in Fig. 6. As already mentioned, the translational and rotational state energies of the photodesorbed NO are positively correlated. The positive correlation between the two DOF suggests their coupling during the desorption process, i.e., they are likely due to a common step in the dynamic sequence. So it contains information on the dynamics and may be influenced by the adsorbate geometry.

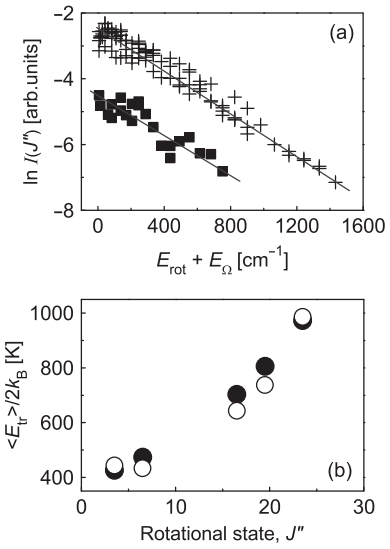

FIG. 8. Absent correlations between (a) rotation and vibration. Rotational plots of NO from 8 nm Ag NPs at $h\nu = 3.5$ eV (*p*-polarization) for $v'' = 0$ (plus signs) and $v'' = 1$ (solid squares). The rotational temperatures are about equal (485 and 497 K, respectively). (b) Translation and vibration. The translational temperatures of photodesorbed NO [same conditions as in (a)] for $v'' = 0$ (solid circles) and $v'' = 1$ (open circles), measured for various rotational states, J''.

On the other hand, as can be seen in Fig. 8(a), the translational and rotational energies do not show any significant change between the $v'' = 0$ and $v'' = 1$ states. Similarly, the rotational distributions of photodesorbed NO are remarkably similar for both vibrational states [see Fig. 8(b)]. This decoupling of the vibrational excitation from the rotational and translational DOF is found for all *D* [including Ag(111)] and all photon energies used in this study. It must be a very basic property of the mechanism.

IV. DISCUSSION

Many aspects of our findings are similar to those reported before for other systems.[3,28] Clearly, we see electronically mediated desorption, with distinct and uneven distributions of energies over the degrees of freedom of the desorbing molecule. Strong predominance of the translation, positive correlation between translation and rotation, and decoupling of the vibration from them, has been seen in many other NO adsorbate systems (see the reviews in Refs. 1–3 and 28). The relative energies going into the various DOF, and even the total energies, vary considerably. For desorption from condensed $(NO)_2$ considerably higher total energies have been reported, with most of it in the vibrations.[31,32] The two spin–orbit-split states were also about equally populated in the desorbing NO in these cases, while in many reports of NO desorption from adsorbed NO monomers on metals

TABLE III. The average translational, rotational, and vibrational energy contents in the photodesorbed NO from "normal" and the fast, new channels (all values are given in eV). Note that the rotational energies may be somewhat underestimated (see text).

Species	Substrate	$\langle E_{tr}\rangle$	$\langle E_{rot}\rangle$	$\langle E_{vib}\rangle$	$\langle E_{tot}\rangle$
Normal at 2.3 eV	4, 8, 10 nm Ag NPs and Ag(111)	0.125	0.04	0.006	0.17
Normal at 3.5 eV	4, 8, 10 nm Ag NPs and Ag(111)	0.125	0.04	0.006	0.17
Normal at 4.7 eV	8, 10 nm Ag NPs and Ag(111)	0.126	0.039	0.006	0.17
Normal at 4.7 eV	4 nm Ag NP	0.126	0.039	0.035	0.20
Fast at 4.7 eV	4 nm Ag NP	0.414	0.055	0.042	0.51

$\langle E_{tr}\rangle$, $\langle E_{rot}\rangle$, and $\langle E_{vib}\rangle$ are the average translational, rotational, and vibrational energies, respectively.

and an oxide[3,28] this was not the case. Since Ref. 3 gives an extensive survey of these results and a thorough discussion of their interpretation, we need not go into details here, but can take over from this in-depth treatise what is directly applicable for the present case. We first briefly summarize the main distinctive aspects of our results reported above, and point out which aspects need discussion. We then go through these points, reaching conclusions where possible.

The detailed data presented on the distributions of energy over the DOF of the photodesorbed NO molecules from $(NO)_2$ adsorbed on silver surfaces show that we can distinguish two regimes, as defined by the sets of DOF energies. The first one, termed "normal" subsequently, is found for all surfaces—from Ag(111) to the smallest NPs— if excitation is induced with 2.3 or 3.5 eV, for the latter also irrespective of polarization (i.e., on and off the plasmon resonance), or by 4.7 eV for Ag(111) and large- to medium-size particles. This shows that in this wide range of varied samples and excitation conditions the intrinsic mechanism does not depend on the excitation mode or on particle properties. In particular, there is no mechanistic difference between excitation on and off the plasmon resonance, even though the desorption cross sections vary widely: a factor of 40 lies between plasmon excitation at the optimum particle size, and excitation at the same energy on Ag(111).[13] The independence of this main channel of the excitation energy must mean that only one excited state is active throughout the range. Also, the fact that 2.3 eV photons suffice to reach this common excited state of PES shows that the energy of the relevant excited state must be lower than this energy. The decoupling of the mechanism from the excitation step and the cross sections had already been deduced in the earlier work[13] using only the translational energy to characterize the mechanism. Corroboration by the full DOF energy distributions strongly supports this conclusion. The data also provide a much more solid ground for discussion of this common intrinsic mechanism.

The second regime becomes detectable for 4.7 eV excitation and small particles; it is already noticeable for somewhat larger particles, and is characterized by higher energies in all DOF compared to the "normal" regime. In particular, the vibrational excitation is considerably enhanced; the positive correlation of translation and rotation persists but with increased gradient. The possibility that the known smaller adsorption energy on small particles[13] simply leads to a shift of the accessed area of the excited PES can be excluded since then the effect should also occur at lower photon energies. This conclusion is also corroborated by the translational distributions (Fig. 5) which suggest two components under these special conditions. The necessity of the higher excitation energy to access this regime shows that a different excited state comes into play. Therefore, this second regime must be characterized by a different mechanism, which possesses a higher energy threshold and is more pronounced for smaller the particles. This implies absence of this new mechanism for desorption from Ag(111), in agreement with experiment.

A. The "normal" regime

In general, photoinduced processes work by the fact that electronically excited states possess PESs with gradients in the Franck–Condon range of the ground state, so that energy is transferred from the electronic system to the nuclei during the lifetime of the excited state, as well as when the system returns to a de-excited state at a different geometry. In photodesorption of adsorbed molecules from metal and semiconductor surfaces, this semiclassical picture is exemplified by semiclassical two-step models, e.g., the MGR (Ref. 5) and Antoniewicz[33] models. A very important point is that the lifetimes of electronically excited states of adsorbates on a metal surface are extremely short (of the order of 1 fs), so that in general the success rate of an excitation is very low for valence excitations.[1–4] An important differentiation of systems is whether the primary excitation is directly induced in the adsorbate (by light absorption or slow electron collision), or whether excitation accumulated in the substrate is transferred onto the adsorbate complex. Usually, the former is found for higher excitation energies, in particular for excitation of localized adsorbate excitations;[4] the latter process dominates at low energies, where the substrate is strongly absorbing and excitations are delocalized. An important specific mechanism here is the transient negative ion (TNI) model.[3,34] According to it, a hot electron produced by photoabsorption in the bulk tunnels into the adsorbate's lowest unoccupied molecular orbital (LUMO). The resulting TNI will, at least for weakly bound species, have a stronger surface bond due to the image potential interaction, so that the adsorbate is accelerated toward the surface accumulating kinetic energy. When the excited electron jumps back into the substrate, the adsorbate will fall back onto the ground state PES at a repulsive position, possibly leading to bond breaking and desorption (Fig. 9). The energy exceeding the bond strength can appear as the desorbate's translational (by center-of-mass acceleration of the adsorbate) and rotational energy (when a torque exists due

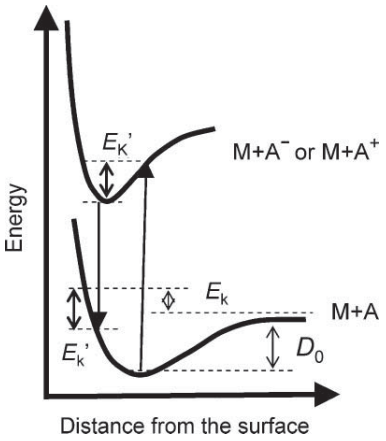

FIG. 9. Sketch of a one-dimensional version of the TNI model, which in the lowest approximation can also be envisaged for the TPI process (*albeit* with a different excited state curve). The ground state (M + A) and excited state ($M + A^+$ or $M + A^-$) curves are indicated, together with some energy differences.

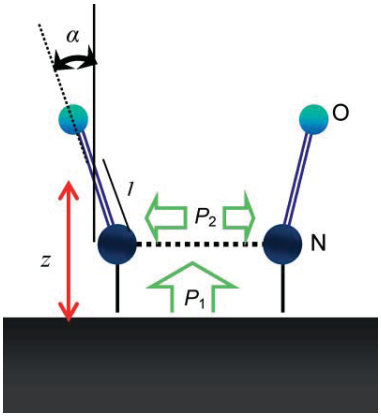

FIG. 10. Sketch of the impulsive model for NO translational and rotational excitation. Momentum transfer from the substrate (P_1) and impulsive rupture of N–N bond (P_2) of the NO dimer can lead to rotationally excited NO.

to the angular situation); the recoil of the desorbed molecule can transfer part of the surplus energy into the substrate. Furthermore, since in most cases the LUMO is antibonding for the adsorbate molecule, the internal bonds will be stretched during the lifetime of the TNI; when the latter is neutralized, energy will remain in the fragment vibrations.

In agreement with earlier work on flat and roughened Ag(111) (Ref. 3 and 11) we have argued before[13,22,23] that this mechanism very likely applies to the photodesorption of NO from $(NO)_2$ on silver surfaces, both on Ag(111) and on Ag NPs. In fact, the persistence of the mechanism indicated by our DOF energy distributions combined with the strong variations of cross sections point to an excitation in the substrate. The TNI mechanism is also supported by the agreement of the calculated position of the $(NO)_2$ π^* unoccupied molecular orbital [$\sim$2 eV above E_F (Ref. 35)] with the photon energy dependence of desorption cross sections.[13,23] Our extensive data on energy distributions support this conclusion as well. Based on the description above, a hot electron created in the Ag substrate will tunnel into the π^* LUMO of an adsorbed $(NO)_2$. The resulting TNI will be accelerated toward the surface; at the same time all bonds will be stretched, since the π^* LUMO is antibonding for both the N-N and N–O bonds of the dimer;[35] in fact the weak N–N bond may already be broken in this regime. When the hot electron tunnels back into the substrate, the evolving complex ends up on the repulsive part of the respective (dimer or monomer, see below) ground state potential. As the system evolves potential energy is transferred to kinetic energy of the fragments.

On Ag surfaces NO adsorbs as a dimer with the N–N axis in the surface plane and an <NNO bond angle of $\sim$120° [Fig. 10].[21] As mentioned above, the bond to the surface, as estimated from the peak temperature[13] of temperature programmed desorption (TPD) is very weak (of the order of 0.1–0.15 eV, i.e., barely larger than the dimer bond;[30]); so the assumption of a more strongly bound TNI is justified. In the impulsive model[3] de-excitation of the TNI dimer (or the evolved complex) to the repulsive region of the dimer ground state PES (or the PES of the fragments) leads not only to acceleration of the center of mass of the complex (and consequently to excitation of the translational DOF) but also to torques which create rotational excitation of the desorbate. If the breaking of the N–N and the surface bond are not happening separately, another possible source for rotational excitation of NO can be the impulsive rupture of the weak N–N bond in a 120° tilted ON–NO configuration of the NO dimer (Fig. 10) after it is de-excited to the ground state PES (Fig. 9) of the dimer; the latter must be connected with the PES of the monomer as we observe desorbing NO monomers. So the main energy transfer to translation and rotation happens upon return into the ground state, on the repulsive part of the corresponding PES. This explains the positive coupling of translational and rotational energies. The absence of coupling to vibrations may be understood within the same model. As noted above, the vibrational excitation of the desorbing molecule stems from the stretching of the adsorbate in the excited state; the energy transferred in this way remains in the molecule when the excitation is transferred back to the substrate, and is converted to vibration of the fragment. Since the translational/rotational excitations mainly result from the evolution on the repulsive part of the ground state, while the vibrations stem from the stretching during the TNI lifetime, these two sets of DOF are decoupled. The predominance of the translational part in the total energy content of the desorbed molecule must stem from the steep gradient of the repulsive potential sampled.

Admittedly, this evolution must be quite complex in the case of the NO dimer, and the discussion here can only be qualitative and approximate as no quantitative theoretical calculations are available. It is likely that the "relevant" neutral PES to which the system reverts after the hot electron has jumped back into the substrate, and on which the main evolution occurs, is at least in part that of the final molecule, the NO monomer. Indeed as mentioned, positive coupling of translation and rotation, and decoupled vibration, have been observed before in many cases of NO monomer desorption.[3,28] They are even seen in molecular beam scattering of NO,[36] in which only the ground state PES is sampled. Obviously a calculation of the ground and excited state PESs and the

evolution of the corresponding wave packet on them would be very interesting. The detailed data reported here would pose a critical test for such calculations. We stress again that in this "normal" regime the influences of MNP properties, including size, are limited to changes of cross sections,[13] i.e., on the attempt rate to this (constant) intrinsic mechanism. The dynamics of the intrinsic mechanism does not at all depend on the size of the NPs, even down to very small particle sizes. This suggests that the PES involved do not change appreciably with NP size; they must even essentially be the same as on Ag(111). This also excludes an important influence of the ground state adsorption energy which does decrease with decreasing particle size, as we showed earlier,[13] or of possible complex adsorption sites on small NPs.

An interesting aspect of our findings, in line with previous observations for NiO,[28] is the small fraction of the total photon energy which ends up as energy content of the desorbing molecule. Together with the energies needed for bond breaking, it amounts to only 10%–20% of the photon energy. The major part is eventually converted to phonons of the substrate. Partly this happens by the recoil in the collision of the molecule with the repulsive PES; most of it probably is connected with the back-transfer of the hot electron in the decay of the TNI, to be eventually converted to phonons of the substrate as well. It should be noted, however, that this heating of the substrate is not sufficient to lead to noticeable thermal desorption. This claim is supported both by the linear dependence of yield on fluence and by estimates of heating (using models as discussed in Ref. 3). It is also corroborated experimentally by the survival of adsorbed N_2O (produced in the photodesorption as well[22]) after photodesorption of all $(NO)_2$, which turns up in post-irradiation TPD to desorb below 120 K.[23]

Our result of equal population of the two spin–orbit-split states differs from many reports for adsorbed monomers, for which different, sometimes *J*-dependent ratios have been seen;[3,28] as mentioned above, it agrees with results for condensed NO dimers[31,32] which, however, differ in other aspects. As discussed in detail in Ref. 3, the populations of these two states can be connected with the rotational axis of the desorbing NO and a possible tilt angle of the adsorbate ground state, the adsorbed monomer. Our result must mean that there is no preferential orientation. We believe that this is connected to the mixing of dimer PESs and (outgoing) monomer PES which destroys any preference. Again, calculations would be helpful.

B. The regime of high excitation energy and small particles

In this regime considerably more energy is transferred to all DOF of the desorbing NO. This is most notable for the translational energy (see Table III and Ref. 13), but can be seen also in the other modes, especially in the vibration. The total energy transferred is about three times larger than in the "normal" regime. As we discussed above, a simple shift of the sampled PES area cannot explain the combination of differences. So a different mechanism has to be considered. To reiterate, the new fast channel is present only for 4.7 eV excitation, and is observable only for small particles.

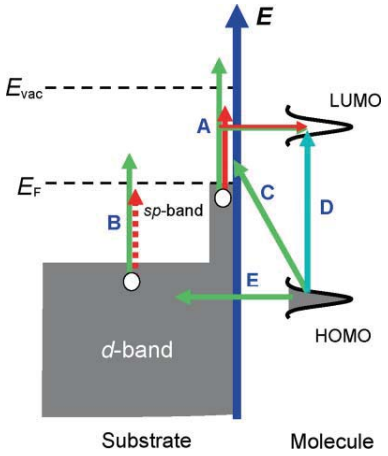

FIG. 11. Schematic view of the various photoexcitation schemes: (A) Excitations to the TNI state (electron transfer from *sp*-band of substrate to the LUMO of the adsorbate), creating a hole in the *sp* band (see text). Short arrow (red): 2.3 or 3.5 eV; long arrow (green): 4.7 eV. (B) Excitation of *d*-band electrons: not possible for 2.3 or 3.5 eV (broken short red arrow); to the empty *sp* states above E_F at 4.7 eV (long green arrow). (C) Direct excitation from occupied adsorbate orbital to the empty *sp*-band of the substrate at 4.7 eV. (D) Direct excitation from HOMO to LUMO of the adsorbate (possibility questionable). (E) Electron transfer from occupied adsorbate state (HOMO) to the *d*-hole created in the excitation mechanism (B) at 4.7 eV (green).

Considering what excitation channels could open up at 4.7 eV but remain closed at 3.5 eV, we see that at the lower photon energy only Ag *s*-electrons can be excited, while at the higher energy also Ag *d*-electrons can be lifted above the Fermi level. This suggests that the new mechanism could be creation of a transient *positive* adsorbate ion (TPI) by tunneling of an electron from the highest occupied molecular orbital (HOMO) of the adsorbate into a surface *d*-hole. This mechanism has been suggested by us before in Ref. 13; a similar suggestion has been made recently for a more complex surface photochemical reaction.[37] Another equivalent process would be a primary charge transfer excitation from the adsorbate HOMO to the empty Ag density of state of the NP. In both cases a TPI in the adsorbate and a (low energy) hot electron in the Ag would result. These processes are depicted in Fig. 11. The TPI would have to evolve such that more energy—in particular more translational energy—would be transferred to the desorbing NO. We have suggested before[13] that this may derive from a closer approach of the TPI to the surface than of the TNI, due to the TPI likely being more compact, as suggested in the original Antoniewicz model for positive ions.[33] Applied to the comparison of TNI and TPI processes, this simple argument assumes that for both TPI and TNI the chemical interaction with the surface is small, so that the corresponding potential energy curves are dominated by the (equal) image charge interaction (Fig. 9). However, we cannot exclude chemical changes as well, which would make this simple argument inapplicable. We also note that 4.7 eV most likely is not sufficient to cause a direct HOMO–LUMO excitation on the adsorbed dimer, although information on the modification of the HOMO–LUMO gap of the dimer (which is about 6 eV in the free molecule[38]) by screening at the Ag surface is lacking. This direct mechanism was suggested for NO desorption from condensed $(NO)_2$ on Ag(111),[31] and

monolayer $(NO)_2$ on LiF(001).[32] Calculational effort to obtain states and PESs concerned would be highly desirable; the detailed data of the DOF energy distributions would be good points of comparison.

We want to point out that both variations of the suggested TPI mechanism do explain why the corresponding channel is strong only in very small particles. With change of the NP size—all other parameters being equal—the number of hot electrons produced scales with the number of Ag atoms in the NP, i.e., $\sim D^3$. Due to the large mean free path of these quasifree *s*-electrons, which considerably exceeds the size of the NPs, all of them can become effective, so that the probability scales with the volume. The number of surface *d*-holes (which are quite immobile), as well as the number of adsorbate molecules, scales with the NP surface area, i.e., $\sim D^2$. So with decreasing particle size the TPI channel (whichever its details) becomes stronger compared to the TNI channel, but the latter stays active as well. We conclude that the combination of necessary excitation energy and predominance in small particles makes the correctness of the suggested TPI mechanism very probable, even though details need theoretical work.

V. SUMMARY AND CONCLUSIONS

In summary, we have investigated the detailed photodesorption dynamics of NO from NO dimers adsorbed on Ag NPs of varied size, supported on alumina films on NiAl(110) substrates with nanosecond laser pulses of 2.3, 3.5, or 4.7 eV, and compared them to the corresponding processes on Ag(111), measured in the same apparatus. Nonthermal desorption which results in translationally and internally hot NO molecules is found. Translational and rotational energies are positively correlated which must be due to a coupled energy transfer mechanism, while the vibrational excitations are decoupled from these modes. These characteristics are found under all conditions of excitation and NP size, from the flat Ag(111) surface to the smallest particles. The confinement of electrons in the NPs and the enhancement of the photodesorption cross section by plasmon excitation, which are known to strongly and size dependently change the desorption cross sections, do not alter the individual desorption dynamics of NO under these "normal" conditions. The findings are well compatible with the earlier conclusion that the common mechanism proceeds via a transient negative ion state. In this model, the coupled translational and rotational excitations of the photodesorbed NO stem from the impulsive interaction of the neutralized TNI on the ground state potential, while the vibrational excitation is the remnant of the stretching of the molecule during its residence time in the TNI. Elucidation of the motion of the desorbing NO on the PESs of dimer and monomer will require calculational effort.

However, for 4.7 eV photons and small NP sizes, a new channel appears in which the desorbing NO carries considerably ($\sim 3\times$) more energy in translation, rotation, and vibration, and which we attribute to a different excitation pathway under these conditions. We argue that this new mechanism proceeds via a transient positive ion which can only be excited at such a high photon energy. These species can be caused either by excitation of *d*-band holes at the Ag NP surface and hole transfer into an adsorbate occupied orbital or by direct charge transfer excitation from the adsorbate HOMO into the Ag NPs *sp*-band above E_F. The increasing contribution of these mechanisms with decreasing size can be explained by the concomitant change of the surface to volume ratio. The detailed information on the energy distributions over the desorbate modes, which must be intimately related to the potential energy surfaces of ground and excited states and the desorption dynamics running on them, should form a good basis for model calculations.

ACKNOWLEDGMENTS

We thank Walter Wachsmann for very able technical assistance and one of the referees for very helpful detailed critique. We acknowledge financial support from the Deutsche Forschungsgemeinschaft within priority program SPP1093 (Dynamik von Elektronentransferprozessen an Grenzflächen), the German–Israeli Foundation (Dynamics of Electronic Processes in a Confined Environment), the Fonds der Chemischen Industrie, and the NEDO International Joint Research Grant on Photon and Electron Controlled Surface Processes.

[1] *Laser Spectroscopy and Photochemistry on Metal Surfaces*, 2 volumes, edited by H.-L. Dai and W. Ho (World Scientific, Singapore, 1995).
[2] X.-L. Zhou, X.-Y. Zhu, and J. M. White, Surf. Sci. Rep. **13**, 73 (1991).
[3] F. M. Zimmermann and W. Ho, Surf. Sci. Rep. **22**, 127 (1995).
[4] For a recent survey, see D. Menzel, Surf. Interface Anal. **38**, 1702 (2006).
[5] D. Menzel and R. Gomer, J. Chem. Phys. **41**, 3311 (1964); P. A. Redhead, Can. J. Phys. **42**, 886 (1964).
[6] See, e.g., H. Guo, P. Saalfrank, and T. Seideman, Prog. Surf. Sci. **62**, 239 (1999); P. Saalfrank, Chem. Rev. **106**, 4116 (2006).
[7] U. Kreibig and M. Vollmer, *Optical Properties of Metal Clusters* (Springer, Berlin, Heidelberg, 1995).
[8] C. F. Bohren and D. R. Huffman, *Absorption and Scattering of Light by Small Particle* (Wiley, New York, 1998).
[9] K. Watanabe, D. Menzel, N. Nilius, and H.-J. Freund, Chem. Rev. **106**, 4301 (2006).
[10] K. B. Myli, S. R. Coon, and V. H. Grassian, J. Phys. Chem. **99**, 16407 (1995).
[11] R. T. Kidd, D. Lennon, and S. R. Meech, J. Chem. Phys. **113**, 8276 (2000).
[12] K. Wettergren, B. Kasemo, and D. Chakarov, Surf. Sci. **593**, 235 (2005).
[13] D. Mulugeta, K. H. Kim, K. Watanabe, D. Menzel, and H.-J. Freund, Phys. Rev. Lett. **101**, 146103 (2008).
[14] P. Christopher, D. B. Ingram, and S. Linic, J. Phys. Chem. C **114**, 9173 (2010).
[15] K. Watanabe, K. H. Kim, D. Menzel, and H.-J. Freund, Phys. Rev. Lett. **99**, 225501 (2007).
[16] K. Watanabe, Y. Matsumoto, M. Kampling, K. Al-Shamery, H.-J. Freund, Angew. Chem. Int. Ed. **38**, 2192 (1998).
[17] C. Voisin, D. Christofilos, N. Del Fatti, F. Vallée, B. Prével, E. Cottancin, J. Lermé, M. Pellarin, and M. Broyer, Phys. Rev. Lett. **85**, 2200 (2000); C. Voisin, D. Christofilos, P. A. Loukakos, N. Del Fatti, F. Vallée, J. Lermé, M. Gaudry, E. Cottancin, M. Pellarin, and M. Broyer, Phys. Rev. B **69**, 195416 (2004).
[18] W. Pfeiffer, C. Kennerknecht, and M. Merschdorf, Appl. Phys. A **78**, 1028 (2004).
[19] V. P. Zhdanov and B. Kasemo, J. Phys.: Condens. Matter **16**, 7131 (2004).
[20] M. Quijada, R. Diez Muino, and P. M. Echenique, Nanotechnology **16**, S176 (2005); M. Quijada, R. Diez Muino, A. G. Borosov, J. A. Alonso, and P. M. Echenique, New J. Phys. **12**, 053023 (2010).
[21] W. A. Brown, P. Gardner, M. Perez Jigato, and D. A. King, J. Chem. Phys. **102**, 7277 (1995); M. P. Jigato, D. A. King, and A. Yoshimori, Chem. Phys. Lett. **300**, 639 (1999).

[22]K. H. Kim, K. Watanabe, D. Menzel, and H.-J. Freund, J. Am. Chem. Soc., **131**, 1660 (2009).
[23]K. H. Kim, Ph.D. dissertation (Freie Universität, Berlin, 2009); K. H. Kim, K. Watanabe, D. Menzel, and H.-J. Freund, (in preparation).
[24]F. Evers, C. Rakete, K. Watanabe, D. Menzel, and H.-J. Freund, Surf. Sci. **593**, 43 (2005).
[25]N. Nilius, N. Ernst, and H.-J. Freund, Phys. Rev. Lett. **84**, 3994 (2000).
[26]K. H. Kim, K. Watanabe, D. Mulugeta, H.-J. Freund, and D. Menzel, Phys. Rev. Lett. (submitted).
[27]D. Mulugeta, Ph.D. dissertation (Freie Universität, Berlin, 2010).
[28]M. Menges, B. Baumeister, K. Al-Shamery, H.-J. Freund, C. Fischer, and P. Andresen, Surf. Sci. **316**, 103 (1994).
[29]G. Herzberg, *Molecular Spectra and Molecular Structure I, Spectroscopy of Diatomic Molecules*, 2nd ed. (Van Nostrand Reinold, New York, 1950).
[30]A. Dkhissi, P. Soulard, A. Perrin, and N. Lacome, J. Mol. Spectrosc. **183**, 12 (1997).
[31]W. C. Natzle, D. Padowitz, and S. J. Sibener, J. Chem. Phys. **88**, 7975 (1988).
[32]R. C. Jackson, J. C. Polanyi, and P. Sjövall, J. Chem. Phys. **102**, 6308 (1995).
[33]P. R. Antoniewicz, Phys. Rev. B **21**, 3811 (1980).
[34]J. W. Gadzuk, L. J. Richter, S. A. Buntin, D. S. King, and R. R. Cavanagh, Surf. Sci. **235**, 317 (1990); R. Franchy, S. K. So, and W. Ho, Vacuum **41**, 284 (1990).
[35]H. Nakamura and K. Yamashita, J. Chem. Phys. **125**, 084708 (2006).
[36]G. D. Kubiak, J. E. Hurst, H. G. Rennagel, G. M. McClelland, and R. N. Zare, J. Chem. Phys. **79**, 5163 (1983); J. Misevich and M. M. T. Loy, J. Chem. Phys. **84**, 1939 (1986).
[37]S. Hagen, P. Kate, F. Leyssner, D. Nandi, M. Wolf, and P. Tegeder, J. Chem. Phys. **129**, 164102 (2008).
[38]A. L. L. East, J. Chem. Phys. **109**, 2185 (1998), and references therein.